Magnetic susceptibility of hot hadronic medium and quark degrees of freedom near the QCD cross-over point

Rupam Samanta^{1,*} and Wojciech Broniowski^{1,†}

¹Institute of Nuclear Physics, Polish Academy of Sciences, 31-342 Cracow, Poland

We argue that the lattice QCD results for the temperature-dependent magnetic susceptibility of the medium below the cross-over temperature are difficult to reconcile with the available hadronic models. In particular, in the widely used Hadron Resonance Gas model, reproducing well numerous other features of the medium, one observes a substantially too strong diamagnetism compared to the lattice simulations. One thus needs a significant source of paramagnetism below the QCD cross-over temperature, possible to achieve with sufficiently light fermions. We thus consider a quark-meson model, where the temperature-dependent quark masses are fixed from the baryon-baryon and baryon-strangeness susceptibility data from the lattice at zero magnetic field. We show that in such a framework one can describe the magnetic susceptibility, with the vacuum contributions duly incorporated. In the hadronic picture, we also evaluate the contribution of the pion-vector-meson loops to the magnetic susceptibility evaluated via the photon polarization, showing it is small and paramagnetic.

I. INTRODUCTION

Magnetic properties of the hot strongly interacting medium have been actively studied on the lattice [1-13]; for recent reviews see [14, 15]. Apart from their fundamental nature, they are associated with very interesting physical phenomena, such as the chiral magnetic effect [16–18], or the magnetic catalysis and inverse catalysis (for a recent review, see, e.g., [19]), reflecting the dependence of the quark condensates on the magnetic field. The information from the lattice QCD at nonzero temperature T, vanishing chemical potentials, and non-zero magnetic field B, involves also properties such as the magnetic field dependent susceptibilities related to various conserved charges (baryon, strangeness, electric) [10, 13], the chiral susceptibilities [20–22], or magnetization [7, 23]. A very basic and relevant quantity is the magnetic susceptibility, χ_B [2, 4, 6, 8, 9], central to this work, as it describes the response of the medium to the magnetic field near B = 0.

It is well known that at vanishing chemical potentials, QCD exhibits a cross-over phase transition [24–27] near the pseudo-critical temperature $T_c \sim 155$ MeV, passing gradually from hadronic degrees of freedom below T_c to quarks and gluons above. The hadronic side is frequently described with the Hadron Resonance Gas model (HRG) [28–31], involving stable hadrons and resonances, mimicking the inter-hadron interactions [32, 33]. HRG reproduces very well many features of hot medium measured on the lattice [34, 35]. In the absence of the magnetic field, the list includes the entropy density, the energy density and pressure, the sound velocity [36–38], the susceptibilities associated to conserved currents and their correlations and cumulants [39–43]. At $0 < B \lesssim 0.15 \; {\rm GeV}^2$ (we use natural units of $\hbar = c = k_B = e = 1$

throughout this paper), conserved charge susceptibilities [10, 13, 44] for $T \sim 150$ MeV are properly reproduced in HRG after the inclusion of the physical magnetic moments of hadrons [45].

With the above successes, HRG became a standard benchmark for the evaluation of thermodynamic quantities in the hadronic phase. Moreover, this is to be linked with the success in the description of the particle yields (see [46] and references herein) in ultra-relativistic nuclear collisions, where statistical hadronization with the chemical freeze-out at $T \sim T_c$ leads to a remarkable agreement of the model with the experimental data. Consequently, a conviction followed that below T_c we deal with just hadrons, and above with quarks and gluons. Certainly, the cross-over nature of the transition makes the division smooth, with hadrons and partons overlapping near T_c , but in practice HRG could be applied up to T_c with a stunning accuracy.

One of the goals of this paper is to point out that there is a notable difficulty in the application of HRG to describe the lattice data for χ_B in the vicinity of T_c . A comparison study was already done in the lattice papers [7, 8] and most recently in [47], but the significance of the vivid mismatch near T_c has not been accentuated, while the agreement between HRG and the lattice at lower T, where the pions largely dominate, was welcome. We try to address this mismatch in the range of T where HRG is expected to be valid, stressing that to be able to describe the lattice data, a suitable model, including the vacuum effects [4, 48], needs to possess sufficient paramagnetism. It also implies that the paramagnetic degrees of freedom in that region must be sufficiently light, not to be damped thermally. Natural candidates here are quarks of constituent masses of a few hundred MeV, appearing in the system from the melt-down of baryons (see, e.g., [49–51].

The methodology applied in this paper is as follows: we use a non-interacting quark-meson model below T_c to describe χ_B , while demanding a simultaneous descrip-

^{*} rupam.samanta@ifj.edu.pl

[†] wojciech.broniowski@ifj.edu.pl

tion of the lattice data for the baryon-baryon $(\chi_{\mathcal{BB}})$ and baryon-strangeness $(\chi_{\mathcal{BS}})$ susceptibilities. The reason for such choice is that (constituent) quarks can provide the needed paramagnetism in the vicinity of T_c , while pions and kaons provide diamagnetism at lower T. Specifically, we use the lattice data for $\chi_{\mathcal{BB}}$ and $\chi_{\mathcal{BS}}$ (at B=0) [43] to find the temperature dependence of the effective quark masses. For these susceptibilities, as we carefully discuss in Sec. III B, in the independent particle approach only the thermal part of the free energy contributes, because the vacuum part does not explicitly depend on the chemical potentials.

With thus obtained temperature-dependent quark masses, and with the pions and kaons present, we compute the subtracted magnetic susceptibility $\chi_B(T) - \chi_B(0)$, as provided by the lattice simulations [8, 47]. The vacuum contributions, which here are relevant, are incorporated. For the quark case, the vacuum part requires a regulator in the spirit of the low-energy effective nonperturbative models [52, 53], which eliminates the contribution of the hard modes. Additionally, we investigate the relevant role of the anomalous magnetic moments of the constituent quarks.

The result of our study is that it is possible to adjust in a natural way the model parameters (the low-energy cut-off, the quark anomalous magnetic moments) such that the quark-meson model, together with the vacuum terms, complies with the data for χ_B and simultaneously with χ_{BB} and χ_{BS} .

The article is organized in the following way. First, in Sec. II, we discuss the lattice results for the conserved charge susceptibilities, $\chi_{\mathcal{B}\mathcal{B}}$ and $\chi_{\mathcal{B}\mathcal{S}}$, and for the magnetic susceptibility, χ_B , and compare them with the state-of-the-art HRG results, pointing out the discrepancy for χ_B . We list the basic definitions of the thermodynamical framework in Sec. III. In Sec. IV, we discuss the basic HRG model and list the formulas for the susceptibilities in the general case with non-zero anomalous magnetic moments. In Sec. V, we consider the quark degrees freedom. The results, obtained within a quark-meson framework and including the vacuum effects, are favorably compared to the lattice data for temperatures near T_c .

For completeness, within HRG we analyze the contribution to χ_B from pion–vector-meson loops. The found paramagnetic effects are small (Sec. VI), at the level of 10-15%, and agree qualitatively with the two-loop Chiral Perturbation Theory [54]. We also point out that the possible role of hadron magnetic polarizabilities to χ_B is tiny (Sec. IV E). More technical issues, in particular, the derivation of the vacuum quark-loop contribution to χ_B , are given in the Appendices.

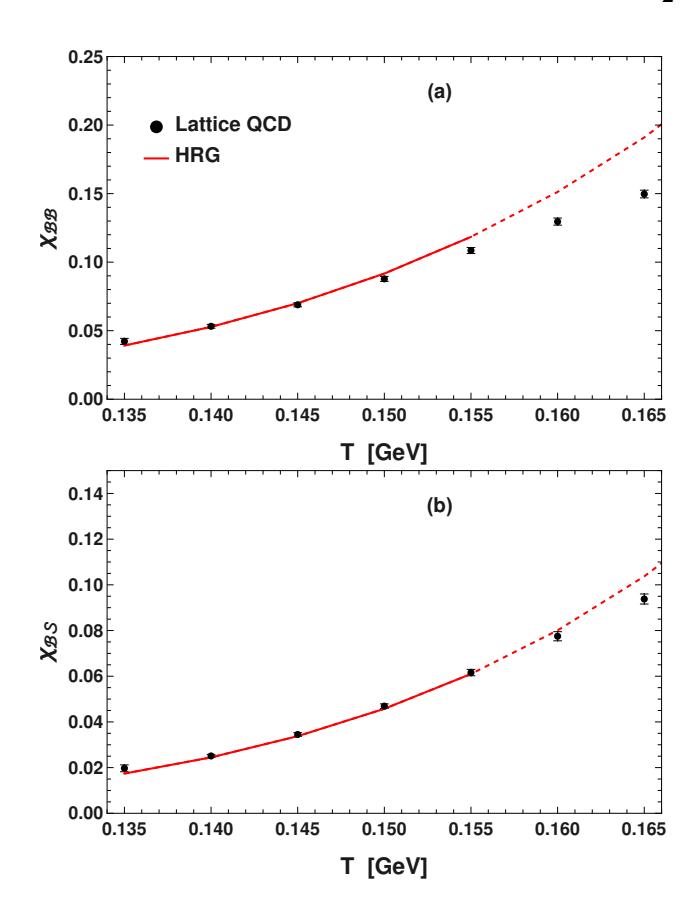


FIG. 1. Susceptibilities $\chi_{\mathcal{BB}}$ and $\chi_{\mathcal{BS}}$ as functions of T, compared to the lattice data [43]. The red solid (dashed) line represents the HRG result below (above) T_c .

II. LATTICE QCD RESULTS FOR SUSCEPTIBILITIES

We begin by presenting the lattice data used in this work as well as the corresponding model results of HRG, deferring the definitions and derivations to the following sections.

The lattice data [43] for χ_{BB} and χ_{BS} are shown in Fig. 1 (the error bars of the data are smaller than the size of the dots). We also display the corresponding HRG results [22, 40, 43], indicated with the lines. Above $T_c \sim 155$ MeV, the lines are dashed to indicate the model is no longer credible there. We note a proper agreement, acclaimed in previous works, for temperatures up to T_c .

The results for $\chi_B(T)$ are displayed in Fig. 2. We show the two most recent determinations from [8] (the photon polarization method) and [47] (the full field method), indicated with the green and orange bands, respectively. The HRG curve matches the lower-temperature end of the lattice data (this was stressed already in [8]), where it is largely dominated by the pions, the lightest hadrons. However, as T increases, HRG falls noticeably below the lattice, remaining large and negative near T_c , where the lattice χ_B crosses zero, changing the behavior from diamagnetic to paramagnetic. Above T_c , outside of the fidu-

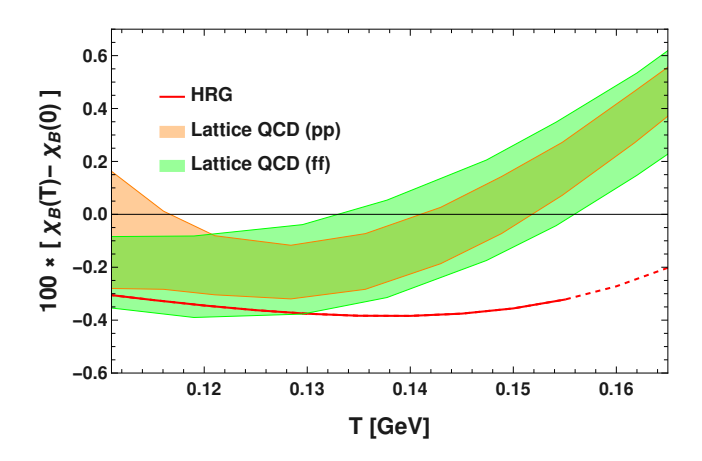


FIG. 2. Magnetic susceptibility χ_B as a function of temperature. The red solid (dashed) line represents the HRG result below (above) T_c . The orange and green bands represent the lattice data obtained using two recent methods: the photon polarization method (pp) [8] and the full field method (ff) [47], respectively.

cial range of HRG ($\lesssim 155$ MeV), the corresponding model curve in Fig. 2 is denoted with dashing.

One should note that the lattice data shown in Fig. 2 involve a rather large extrapolation to the physical point of $m_{\pi}=140$ MeV. The applied methodology in [8, 47] has improved on the earlier results [6, 7], where χ_B was actually positive in the whole probed range of T>100 MeV (cf. Fig. 4 in [8]). While the mismatch between the model and the lattice data displayed in Fig. 2 remains within the 2σ uncertainty, it is persistent in the wide range of T, which we assess as a symptom of a genuine effect.

We also stress that χ_B , being the curvature of the pressure (the partition function) at B=0 (see Sec. III), is a low-B feature. Therefore, its evaluation in the hadronic phase avoids the complications due to a possible modification of the hadronic structure and the resonances at strong B [55, 56], casting doubt on the validity of HRG [57]. The failure of reproducing such a basic quantity within HRG, at temperatures where it has been traditionally used, urges one to rethink the composition of the hadronic medium below T_c , in search of a paramagnetic component. Moreover, the vacuum contributions, explicit in χ_B but not treated in HRG, need to be considered (see Sec. III B).

III. THERMODYNAMICS IN A MAGNETIC FIELD

A. Basic definitions

Thermodynamical properties of a system treated via the grand canonical ensemble can be obtained from the the grand thermodynamical potential density Ω [58, 59], which in the presence of a magnetic field is

$$\Omega = U - TS - B\mathcal{M} - \mu N,\tag{1}$$

where U is the internal energy, S - the entropy, \mathcal{M} - magnetization, and $\mu N = \mu_{\mathcal{B}} \mathcal{B} + \mu_{\mathcal{S}} \mathcal{S} + \dots$ involves the combination of chemical potentials and the corresponding conserved charges.¹ In the thermodynamic limit of a large volume, Ω is related to the system pressure, $P = -\Omega/V$.

The conserved charge susceptibilities used in this work are defined as

$$\chi_{\mathcal{B}\mathcal{B}} = \frac{1}{T^2} \frac{\partial^2 P}{\partial \mu_{\mathcal{B}}^2} \Big|_{\mu_{\mathcal{B},S}=0}, \quad \chi_{\mathcal{B}S} = \frac{1}{T^2} \frac{\partial^2 P}{\partial \mu_{\mathcal{B}} \partial \mu_{\mathcal{S}}} \Big|_{\mu_{\mathcal{B},S}=0}. (2)$$

They are evaluated at vanishing chemical potentials, as in lattice QCD.

According to Eq. (1), the magnetization density of the system is obtained as

$$\mathcal{M} = \frac{\partial \mathcal{P}}{\partial B},\tag{3}$$

while the magnetic susceptibility is given by the second derivative of the pressure at B=0,

$$\chi_B = \frac{\partial \mathcal{M}}{\partial B} \bigg|_{B=0} = \frac{\partial^2 P}{\partial B^2} \bigg|_{B=0}.$$
(4)

Generically, the pressure can be decomposed into the thermal and vacuum parts, $P = P^{\rm th} + P^{\rm vac}$. In the non-interacting particle picture, such as HRG or the quark-meson model studied later, at B=0 the thermal part for an individual particle species (for brevity, we omit indexing of the particle species below) has the form

$$P^{\text{th}} = -\eta T \sum_{s_z} \int \frac{d^3 p}{(2\pi)^3} \log[1 - \eta f(E_p, T, \mu)], \quad (5)$$

where $f(E_p, T, \mu)$ represents the occupation number of a stable hadron or a resonance with a given statistics,

$$f(E_p, T, \mu) = \frac{1}{\exp(\frac{E_p - \mu}{T}) + \eta}.$$
 (6)

Here $E_p = \sqrt{m^2 + p^2}$ denotes the energy, s_z is the spin projection, and $\eta = +1$ or -1 depending whether the particle is a fermion or a boson. The corresponding vacuum part can be formally written as [4]

$$P^{\text{vac}} = -\frac{1}{2}\eta \sum_{a} \int \frac{d^3p}{(2\pi)^3} E_p,$$
 (7)

which is infinite, thus requires regularization, to be discussed later and detailed in Appendix B.

In the presence of a magnetic field $\vec{B} = B\hat{z}$, for charged particles the corresponding formulas involve a sum over

¹ To distinguish the baryon number from the magnetic field, we use \mathcal{B} for the former, and B for the latter.

the Landau levels l [58, 59]

$$P^{\text{th}} = -\eta T \frac{B|Q|}{2\pi^2} \sum_{l=0}^{\infty} \sum_{s_z} \int_0^{\infty} dp_z \log[1 - \eta f(p_z, B)],$$

$$P^{\text{vac}} = -\eta \frac{B|Q|}{4\pi^2} \sum_{l=0}^{\infty} \sum_{s} \int_0^{\infty} dp_z E(p_z, B).$$
(8)

For the neutral particles, equations of the form (5,7) hold, but E may explicitly depend on B if the particle has an anomalous magnetic moment (cf. Sec. IV A).

B. Self-consistency

From the above expressions, it is apparent that in the independent particle picture, the decomposition of the pressure into the thermal and vacuum parts involves functions of the following arguments:

$$P = P^{\text{th}}(T, \mu, B; \{m\}) + P^{\text{vac}}(B; \{m\}), \tag{9}$$

where $\{m\}$ denotes the collection of masses of particles. Since the energy spectrum of particles and antiparticles is the same due to the charge conjugation symmetry, we have the feature

$$P^{\text{th}}(T, \mu, B; \{m\}) = P^{\text{th}}(T, -\mu, B; \{m\}),$$
 (10)

i.e., the symmetry in μ . Note that the vacuum term does not explicitly depend on the thermal parameters.

The masses may depend on the thermal parameters and B, namely $\{m\} = \{m(T, \mu, B)\}$, bringing additional implicit dependence in P. In various effective models, P is treated as an effective potential for the determination of masses (or other quantities). The self-consistency condition is

$$\frac{\partial P}{\partial m} = 0. \tag{11}$$

Note that thus obtained mass must be a symmetric function of μ , as implied by the property (10). In particular,

$$\partial m/\partial \mu \mid_{\mu=0} = 0.$$
 (12)

It is now instructive to evaluate various quantities needed in this work. The baryon density is

$$\mathcal{B} = \frac{dP}{d\mu_{\mathcal{B}}} = \frac{\partial P}{\partial \mu_{\mathcal{B}}} + \frac{\partial P}{\partial m} \frac{\partial m}{\partial \mu_{\mathcal{B}}} = \frac{\partial P^{\text{th}}}{\partial \mu_{\mathcal{B}}},\tag{13}$$

where (11) was used. For the susceptibility,

$$\chi_{\mathcal{B}\mathcal{B}} = \frac{1}{T^2} \left. \frac{d^2 P}{d\mu_{\mathcal{B}}^2} \right|_{\mu_{\mathcal{B}}=0} = \frac{1}{T^2} \left[\frac{\partial^2 P}{\partial \mu_{\mathcal{B}}^2} + \frac{\partial P}{\partial m} \frac{\partial^2 m}{\partial \mu_{\mathcal{B}}^2} \right.$$

$$\left. + 2 \frac{\partial^2 P}{\partial m \partial \mu_{\mathcal{B}}} \frac{\partial m}{\partial \mu_{\mathcal{B}}} + \frac{\partial^2 P}{\partial m^2} \left(\frac{\partial m}{\partial \mu_{\mathcal{B}}} \right)^2 \right]_{\mu_{\mathcal{B}}=0}$$

$$= \frac{1}{T^2} \left. \frac{\partial^2 P^{\text{th}}}{\partial \mu_{\mathcal{B}}^2} \right|_{\mu_{\mathcal{B}}=0}, \tag{14}$$

where we have used conditions (11) and (12). An analogous equality follows for χ_{BS} :

$$\chi_{\mathcal{B}S} = \frac{1}{T^2} \left. \frac{\partial^2 P^{\text{th}}}{\partial \mu_{\mathcal{B}} \partial \mu_S} \right|_{\mu_{\mathcal{B},S} = 0}.$$
 (15)

The meaning of Eqs. (13-15), despite the simplicity of the derivation, is sound, as (in the independent particle approach) it allows one for a "naive" evaluation of these quantities just from the thermal part. The vacuum term manifests itself only indirectly through the self-consistency conditions, in general leading to T, μ , or B-dependent particle masses.

For the magnetization and the magnetic susceptibility, derived using Eqs. (3) and (4), the situation is entirely different, since both the thermal and the vacuum parts depend explicitly on the magnetic field.² Thus also the vacuum contributes directly to \mathcal{M} and χ_B and needs to be considered [4, 48]. This makes the modeling of these magnetic features much more demanding, as it is prerequisite to model the vacuum part of P.

IV. HADRON RESONANCE GAS

A. Energy spectra

In HRG, one deals with a non-interacting system of stable hadrons and resonances, which incorporate in a simplified way the interactions between the stable hadrons [28–33, 36, 60].

The energy spectra of individual hadrons in a magnetic field depend on their spin. The relevant formulas were reviewed in [45]. In particular, for spin-0 charged states (e.g., π^{\pm} , K^{\pm}),

$$E \equiv \epsilon_{l,p_z} = \sqrt{M^2 + p_z^2 + B|Q|(2l+1)},$$
 (16)

where Q denotes the particle electric charge and l labels the Landau level.

For spin- $\frac{1}{2}$ particles with an anomalous magnetic moment κ , one has the Tsai-Yildiz formula [61]

$$\epsilon_{l,p_{z}} = \sqrt{\left(\sqrt{M^{2} + B\left[|Q|(2l+1) - 2Qs_{z}\right]} - 2\mu_{M}B\kappa s_{z}\right)^{2} + p_{z}^{2}},$$
(17)

for states of non-zero charge Q (such as the proton), and

$$\epsilon_{p,p_z} = \sqrt{\left(\sqrt{M^2 + p^2 - p_z^2} - 2\mu_M B \kappa s_z\right)^2 + p_z^2}$$
 (18)

² The explicit dependence of $P^{\rm th}$ and $P^{\rm vac}$ on B originates simply from the explicit dependence of the energy spectrum on B, as discussed in detail in Sec. IV A.

for neutral states (such as the neutron). Here $\mu_M = \frac{1}{2M}$ is the natural magneton of the particle. Our convention for the gyromagnetic ratio of the hadron is

$$g = 2(Q + \kappa). \tag{19}$$

For higher spin states we adopt the same prescription as in [45], where the anomalous magnetic moments of hadrons are treated non-relativistically as small corrections. For instance, in case of spin-1 or spin- $\frac{3}{2}$ (Rarita-Schwinger) charged states [62] (e.g., ρ or Δ), we use [45]

$$\epsilon_{l,p_z} = \sqrt{M^2 + p_z^2 + B[|Q|(2l+1) - 2Qs_z]} - 2B\mu_M \kappa s_z,$$
(20)

and for particle with spin larger than $\frac{3}{2}$, we treat the entire spin interaction non-relativistically [45],

$$\epsilon_{l,p_z} = \sqrt{M^2 + p_z^2 + B|Q|(2l+1)} - gB\mu_M s_z.$$
 (21)

With the above spectra one can obtain the pressure for individual hadron species (8), which then can be used to obtain the susceptibilities. In our study, we use QMHRG2020 – an augmented list of hadrons including some additional quark-model states, that properly reproduces the conserved charge susceptibilities at B=0 [10, 43, 45]. For a thorough discussion of variants of HRG see, e.g., [63]. The values of κ used in the calculations presented in this paper are taken from Table I compiled in [45].

B. Baryon-baryon and baryon-strangeness susceptibilities

As shown in Sec. III B, for $\chi_{Q_1Q_2}$ only the thermal part of the pressure contributes directly. Using Eq. (2), one obtains a generic expression³

$$\chi_{Q_1Q_2} = \frac{Q_1Q_2(2s+1)}{2\pi^2T^2} \int_0^\infty dp \left(m^2 + 2p^2\right) \frac{f(E_p)}{E_p}, (22)$$

where $Q_i = \mathcal{B}$ or S, s is the particle's spin, and $f(E_p) \equiv f(E_p, T, \mu = 0)$.

Summing over the particle species, we readily obtain χ_{BB} and χ_{BS} in HRG. Fig. 1 shows the results from HRG, compared to the lattice data [43]. It is seen that HRG is successful in describing the lattice data both qualitatively and quantitatively up to $T_c \sim 155$ MeV. Above T_c , one observes a gradual deviation, typically attributed to an emergence of the QCD degrees of freedom.

C. Magnetic susceptibility with anomalous magnetic moments

In HRG, one considers only the thermal part of the magnetic susceptibility. Some details of the straightforward derivations of the following formulas are given in Appendix A).

For the diamagnetic component one gets

$$\chi_B^{\text{dia}} = -\frac{Q^2(2s+1)}{24\pi^2} \int_0^\infty dp \, \frac{f(E_p)}{E_p},\tag{23}$$

which is clearly negative-definite and monotonic for each particle.

The form of the paramagnetic component depends on the spectrum used. For spin- $\frac{1}{2}$ particles with the Tsai-Yildiz expression (17), one gets (see Appendix A)

$$\chi_{B;s=\frac{1}{2}}^{\text{para}} = \frac{s(s+1)(2s+1)}{6\pi^2} \int_0^\infty dp \times \left[Q^2 + 2Q \kappa + \left(1 + \frac{p^2}{m^2} \right) \kappa^2 \right] \frac{f(E_p)}{E_p}. \quad (24)$$

The cases corresponding to spectra of Eqs. (20,21) used for higher spin states are listed in Appendix A. Obviously, all are positive-definite. In the limit of a large mass m, all the expressions reduce to the formula

$$\chi_{B;m\gg T}^{\text{para}} = \frac{s(s+1)(2s+1)g^2}{24\pi^2} \int_0^\infty dp \frac{f(E_p)}{E_p}, (25)$$

becoming proportional to the gyromagnetic factor squared. The sum $\chi_B^{\rm dia} + \chi_B^{\rm para}$ is positive for any s>0 state and monotonic.

From the formulas for χ_B^{para} it is clear that, as expected, the inclusion of the anomalous magnetic moments enhances the paramagnetic component of the magnetic susceptibility in HRG. However, with the physical κ 's, the total enhancement effect is mild, as can be seen from the comparison in Fig. 3. We recall that the inclusion of the physical κ 's, which are large for baryons, was crucial to achieve agreement for the conserved charge susceptibilities in HRG at nonzero values of B [45]. In Fig. 3, the HRG curves above T_c are dashed, to indicate they only carry a formal meaning there. At lower values of T, the relative effect of κ decreases, to become $\sim 15\%$ of the total χ_B at T=140 MeV. Hence the mismatch between HRG results (obtained from the thermal part of the pressure) and the lattice persists even after including the anomalous magnetic moments. We note that in Figs. 2 and 4 the results labeled "HRG" include the anomalous magnetic moments.

D. Anatomy of the magnetic susceptibility

In order to better understand the HRG results, in Fig. 4 we show the contributions from the dominating

³ It simply follows from the fact that $f(1 - \eta f) = -T df/dE_p$ and an integration by parts.

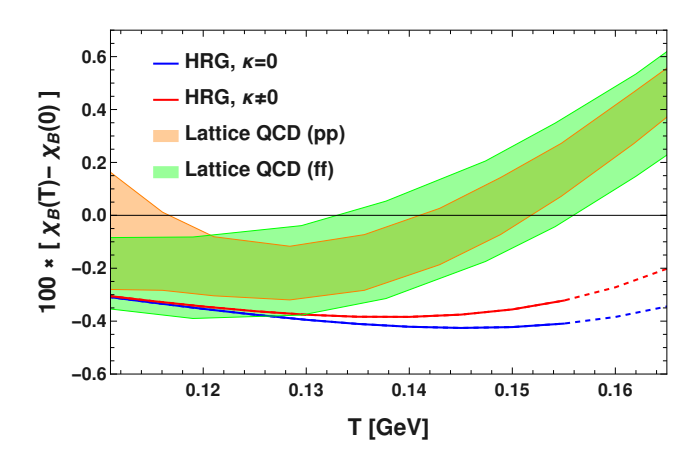


FIG. 3. Magnetic susceptibility as a function of temperature, calculated in the HRG model including (red) and excluding (blue) the anomalous magnetic moments of hadrons. The lines above T_c are dashed. The orange and green bands show the lattice data as in Fig. 2.

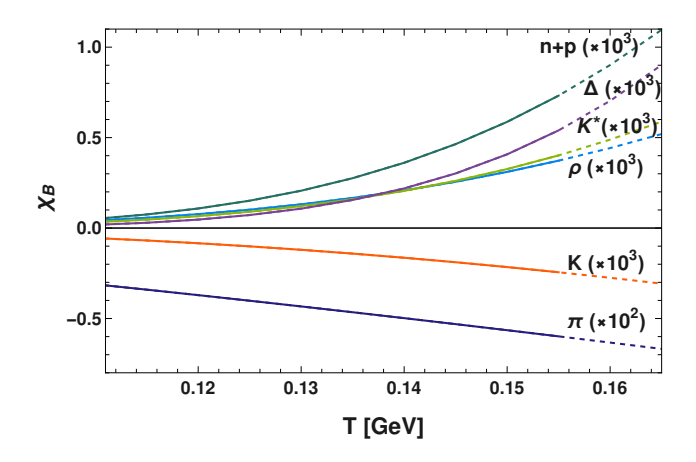


FIG. 4. Magnetic susceptibility of several hadron species as functions T. The numbers in parenthesis next to labels denote factors by which a given result is multiplied. The hadron labels include the antiparticles and the spin-isospin degeneracy.

hadron species plotted as functions of T. The numbers in parenthesis next to the label of each curve denote a factor by which the given result is multiplied, which is 10^2 for the pion and 10^3 for the other hadrons. The result for each curve includes the corresponding anti-particles, as well as the spin and isospin (charge) degeneracy.

The magnitude of χ_B for each hadron species, naturally, grows with the increasing temperature for both the paramagnetic and diamagnetic cases. It is controlled by the mass of the hadron through the occupation number via the formulas from Sec. IV C and Appendix A), which at large masses are damped as $e^{-M/T}$. Thus, at lower values of T higher mass hadrons are strongly suppressed and one is left with the leading diamagnetic contribution of the pion. As T increases, the kaons join the diamagnetic contribution. As a result, at temperature range $135~{\rm MeV} < T < 165~{\rm MeV}$, the nature of HRG remains

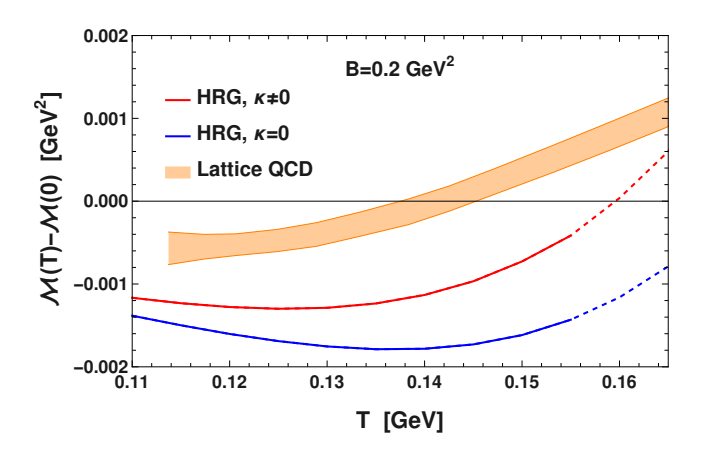


FIG. 5. Subtracted magnetization, $\mathcal{M}(B,T) - \mathcal{M}(B,0)$, at $B = 0.2 \text{ GeV}^2$, plotted as a function of T. The lattice result, obtained from the data from [7], is represented with the orange band. The blue and red curves represent, respectively, the HRG results without and with the anomalous magnetic moments of hadrons.

diamagnetic. At higher values of T other states appear, bringing in paramagnetic contributions, mostly from the numerous baryonic states of higher mass [64], which actually at large $T\sim 170~{\rm MeV}>T_c$ (well outside of the expected validity of HRG) prevail over the diamagnetic terms.

E. Magnetic polarizabilities of hadrons

An external constant and uniform magnetic field induces deformation of a composite object, whose dynamical response (at T=0) is quantified with the magnetic polarizability. To quadratic order, the energy picks up a contribution

$$\Delta E = -\frac{1}{2}\beta B^2,\tag{26}$$

where β is the polarizability of the hadron. The estimates are $\beta_{\pi^{\pm}} \sim -2 \times 10^{-4} \text{ fm}^3$ [65], $\beta_{\pi^0} \sim 3 \times 10^{-4} \text{ fm}^3$ [66], $\beta_n \sim 4 \times 10^{-4} \text{ fm}^3$ [67], and $\beta_p \sim 2 \times 10^{-4} \text{ fm}^3$ [67]. The term (26) in the definition of χ_B would yield an extra piece for a particle species,

$$\chi_B^{\text{pol}} = \frac{\beta}{2\pi^2} \int_0^\infty dp \ p^2 \ f(E_p),$$
(27)

which is proportional to the density of states at B=0. With the above-quoted values for β 's, we find that $100\chi_B^{\rm pol} \sim -0.002$, negligible compared to the values in Fig. 4.

F. Magnetization

To corroborate the qualitative findings for χ_B , we also examine the magnetization \mathcal{M} of Eq. 3. This quantity

depends on the magnitude of magnetic field B, which here we set to $B=0.2~{\rm GeV}^2$, sizable but not too large to avoid the problems for hadrons in a too strong magnetic field [45, 55, 56]. Since \mathcal{M} needs subtraction due to the vacuum contribution [4], we plot this quantity subtracted at T=0, namely $\mathcal{M}(B,T)-\mathcal{M}(B,0)$. Note that the possible vacuum contribution is absent in HRG, similar to the case of χ_B .

Figure 5 shows the results for the subtracted magnetization in HRG compared with lattice data [7]. We observe a qualitatively similar feature as in χ_B , namely a too strong diamagnetism in HRG, placing the model curve way below the data. The effect of the anomalous magnetic moments of hadrons on $\mathcal{M}(B,T)-\mathcal{M}(B,0)$ is moderate.

V. QUARK DEGREES OF FREEDOM

A. Motivation

In the previous sections we have argued that within HRG it is not possible to achieve agreement with the lattice results for $\chi_B(T)$ in the fiducial temperature range. A general conclusion is that one needs states with s>0 and of sufficiently low mass, such that at $T\sim T_c$ their paramagnetism may overcome the diamagnetism from the pions and kaons. Obvious candidates here are the (constituent) quarks, which as spin- $\frac{1}{2}$ states are paramagnetic and light enough. Moreover, the inclusion of quarks allows one to model the needed vacuum term, advocated in Sec. III B.

As seen from the lattice data, we also need to retain the diamagnetism at low values of T, where $\chi_B(T)$ is negative. For that reason we shall keep the pions and kaons as additional degrees of freedom, in the spirit of the quark-meson models (see [68] and references therein). Thus, we consider an independent particle model with constituent quarks of three colors and flavors, pions, and kaons. Recently, quark meson models at non-zero B have been in similar tasks in [48, 69, 70].

B. Temperature-dependent quark masses from fits to χ_{BB} and χ_{BS}

We fix the quark masses as functions of T from the requirement to describe the lattice data for $\chi_{\mathcal{B}\mathcal{B}}$ and $\chi_{\mathcal{B}\mathcal{S}}$ from [43] shown in Fig. 1. We use here Eqs. (14) and (15) and consider equal mass for u and d quarks, denoted by $m_l = m_u = m_d$, and an independent strange quark mass m_s . The procedure goes as follows: First, $m_s(T)$ is fitted to the $\chi_{\mathcal{B}\mathcal{S}}$ data at each value of T, according to Eq. (15) where only the strange quarks contribute. Then, we use thus obtained $m_s(T)$ to fix $m_l(T)$ with the $\chi_{\mathcal{B}\mathcal{B}}$ data, according to Eq. (14), where the quarks of all three flavors contribute.

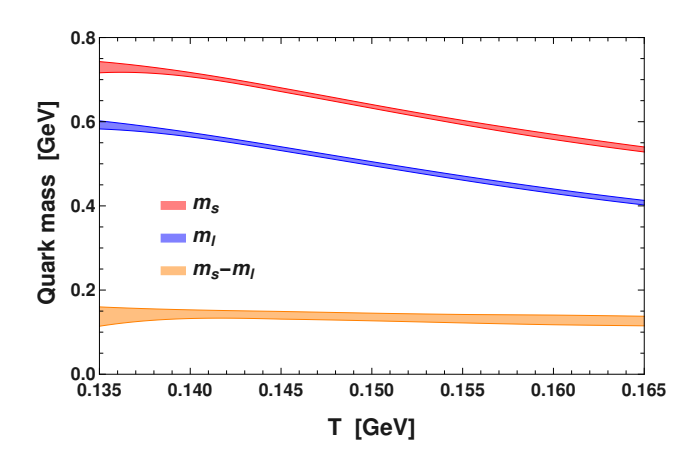


FIG. 6. Light and strange quark masses as functions of T from the fit to the lattice data for $\chi_{\mathcal{B}\mathcal{B}}$ and $\chi_{\mathcal{B}\mathcal{S}}$ of Fig. 1 (blue and red bands, respectively), and the difference $m_s - m_l$ (orange band). The width of the bands reflects the uncertainty of the lattice data [43].

The above methodology is analogous to the one from [71], where the entropy density was used to find the *T*-dependence of constituent quarks and gluons, termed as quasiparticles [72].

The obtained result for the quark masses is presented in Fig. 6. First, we note that at $T \sim T_c$ they are significantly larger than the traditional constituent masses, where $m_l \sim 300$ MeV, but, interestingly, are in the ballpark of the quasiparticle masses of Fig. 2 in [71], where $m_l(T_c) \sim 550$ MeV and $m_s(T_c) \sim 600$ MeV. Second, the splitting $m_s - m_l$ in our Fig. 6 is remarkably stable in the displayed range of T, being around 120–130 MeV, which is typically expected in the constituent quark picture.

C. Vacuum contribution

As discussed in Sec. III B, the vacuum contribution to the pressure depends explicitly on B via the energy spectrum, therefore making it important for the evaluation of χ_B . In the quark-meson model, the vacuum terms were computed in [48], with dimensional regularization and renormalization applied. For the quarks, the vacuum contribution to χ_B can be evaluated according to the diagram of Fig. 7, representing the photon polariza-

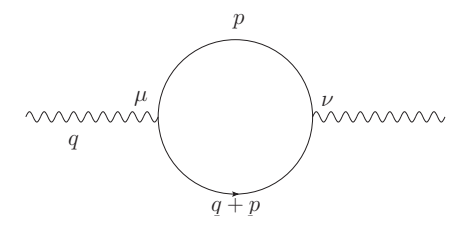


FIG. 7. Photon vacuum polarization diagram for quarks

tion $\Pi^{\mu\nu}$. We use the formula (see, e.g., [4, 9, 73, 74])

$$\chi_B^{q,\text{vac}} = \frac{1}{2} \lim_{\vec{q} \to 0} \lim_{q_0 \to 0} \frac{\partial^2 \text{Re}[\Pi_s^{q,\text{vac}}]}{\partial q^2}, \tag{28}$$

with q_0 and \vec{q} denoting the photon's momentum and $\Pi_{s,\mathrm{vac}}^{q,\mathrm{vac}} = \frac{1}{2} \sum_{i=1}^{3} \Pi_{ii}^{q,\mathrm{vac}}$.

Here, in the spirit of effective quark models, rather than carrying out the renormalization procedure, we apply a regulator and keep it to remove the hard-momentum contributions. Specifically, we use Pauli-Villars regularization scheme with two-subtractions [52, 53], as given by Eq. (B6). We also incorporate the possible anomalous magnetic moments of the constituent quarks, taking the vertex in the form [61, 75–77]

$$\Gamma^{\mu} = Q\gamma^{\mu} + \frac{\kappa}{2m}\sigma^{\mu\nu}q^{\nu} \tag{29}$$

(see Appendix B for details).

With the described procedure we find explicitly for each quark species (treating color separately)

$$\begin{split} \chi_B^{q,\text{vac}}(T) &= \frac{Q^2}{36\pi^2} \left(\frac{2\Lambda^4 + 3\Lambda^2 m^2}{(\Lambda^2 + m^2)^2} - 3\log[\frac{\Lambda^2}{m^2} + 1] \right) \\ &+ \frac{\kappa Q}{4\pi^2} \left(\log[\frac{\Lambda^2}{m^2} + 1] - \frac{\Lambda^2}{\Lambda^2 + m^2} \right) \\ &+ \frac{\kappa^2}{48\pi^2} \left(\Lambda^2 (\frac{4}{\Lambda^2 + m^2} - \frac{1}{m^2}) - 3\log[\frac{\Lambda^2}{m^2} + 1] \right), \end{split}$$

where $\Lambda \sim 800$ MeV is the scale of the regulator and m = m(T) is the temperature-dependent quark mass.⁴

For the mesons, one can compute the pion (or kaon) loop in the photon vacuum polarization diagram (see Fig. 10). The leading term, renormalized to 0 at T=0, is [48]

$$\chi_B^{\text{mes,vac}}(T) - \chi_B^{\text{mes,vac}}(0) = -\frac{1}{48\pi^2} \log \left[\frac{m(0)}{m(T)} \right], \quad (31)$$

where now m(T) denotes the temperature dependent pion or kaon mass. Numerous lattice and model studies suggest that these masses grow very slowly up to $\sim T_c$, where they starts to increase rapidly.

D. Quark anomalous magnetic moments

The quark anomalous magnetic moments are estimated from a non-relativistic quark model calculation of the baryon magnetic moment μ_p , μ_n , and μ_{Λ^0} , using [75, 78–80]

$$\mu_{p} = \frac{4}{3}\mu_{u} - \frac{1}{3}\mu_{d},$$

$$\mu_{n} = \frac{4}{3}\mu_{d} - \frac{1}{3}\mu_{u},$$

$$\mu_{\Lambda} = \mu_{s}.$$
(32)

We solve the above equations with the physical values of the baryon magnetic moments (collected, e.g., in Table-I of [45]). The result is, $\mu_u=1.852~\mu_N,~\mu_d=-0.972~\mu_N,$ and $\mu_s=-0.613~\mu_N$. We then apply Eq. (19) to get κ_q 's.

E. Magnetic susceptibility

The full magnetic susceptibility in the quark-meson model is composed as follows:

$$\chi_B(T) = N_c \sum_{u,d,s} \left[\chi_B^{q,\text{th}}(T) + \chi_B^{q,\text{vac}}(T) \right]$$

$$+ \sum_{\pi K} \left[\chi_B^{\text{mes,th}}(T) + \chi_B^{\text{mes,vac}}(T) \right].$$
 (33)

In this formula, the quark and meson masses are temperature-dependent. For the quark case, we take the dependence found in Sec. VB in the available range of T, while for $m_{\pi}(T)$ and $m_{K}(T)$ we use the model results from the quark-meson model given in Fig. 3 of [48].

Since the lattice data [9, 47] correspond to the subtraction $\chi_B(T) - \chi_B(0)$, we do the same in the quark meson model. The thermal parts vanish at T=0, the vacuum meson part of Eq. (31) is already subtracted, whereas for the subtraction of the quark vacuum part we would need the quark masses at T=0. However, these are inaccessible to the method of Sec. VB, since the lattice data for $\chi_{\mathcal{B}\mathcal{B}}$ and $\chi_{\mathcal{B}S}$ at T=0 are not available. Thus we first probe several reasonable values for $m_l(0)$ and $m_s(0) = m_l(0) + 120$ MeV, and later use a different subtraction scheme.

In panel (a) of Fig. 8 we present the results for $\chi_B(T) - \chi_B(0)$ obtained with the described procedure, probing several values of $m_l(0)$. We note that a reasonable agreement to the lattice data is achieved with $m_l(0) = 600$ MeV. We compare the cases with and without the quark anomalous magnetic moments in panel (b), drawing the conclusion that the role of the quark anomalous magnetic component is significant, as it raises the paramagnetic component. Finally, in panel (c) we present the decomposition of $\chi_B(T) - \chi_B(0)$ into various components described in the legend. All the curves start at T = 135 MeV, as this is the lower limit for the data of Fig. 6.

The vacuum contribution of the quarks is negative. It remains flat at low T, and above $T \sim 155$ MeV starts to decrease more rapidly. The small mesonic vacuum contribution is positive and remains essentially constant for the entire temperature range. The thermal contribution for the quarks is strongly paramagnetic and increases monotonically with temperature, while the thermal contribution of the mesons is diamagnetic and does not vary much in the considered range of T (reflecting the mild growth of m(T) for T below T_c [48]).

The overall conclusion from Fig. 8 is that the considered quark-meson framework is capable of explaining the

⁴ For the $\kappa=0$ case, taking the limit $\Lambda\to\infty$ and subtracting the T=0 yields the same renormalized formula as in [48].

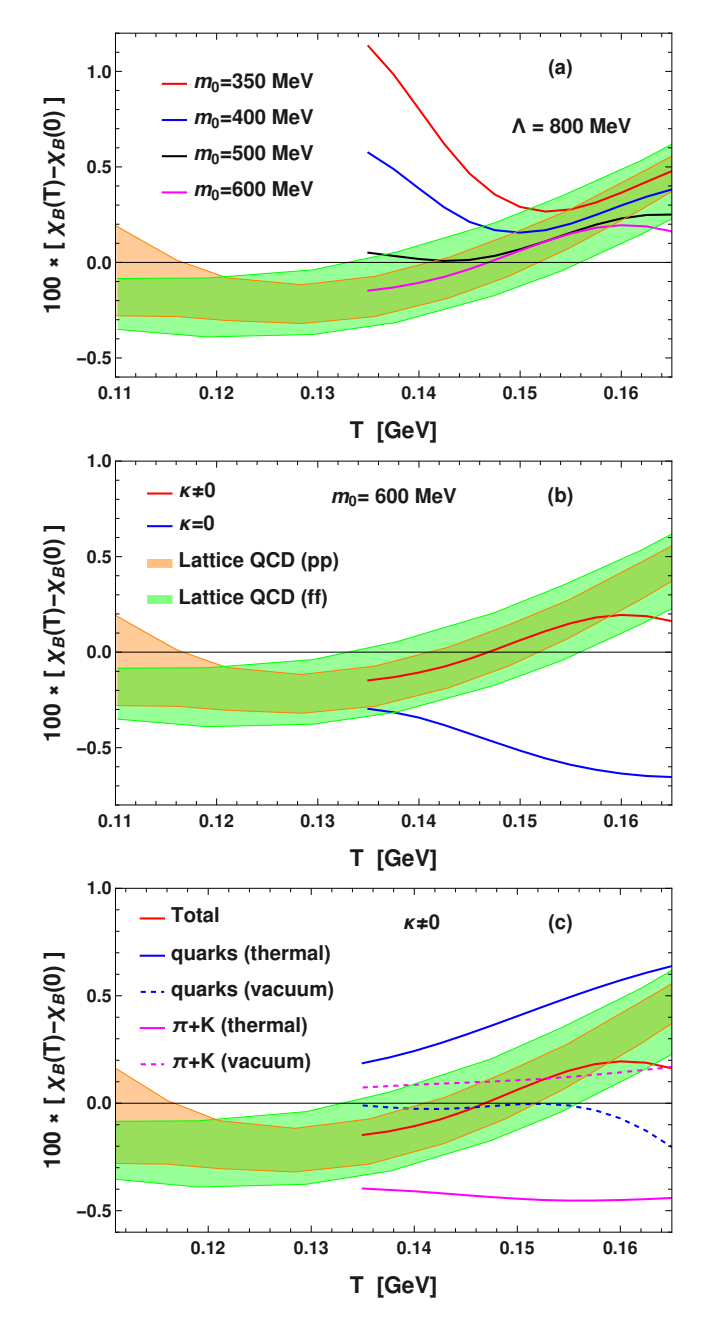


FIG. 8. (a) Magnetic susceptibility as a function of T in the quark-meson model with fitted quark masses from Fig. 6 and temperature dependent meson masses from [48]. The results include both the thermal and vacuum parts with non-zero quark anomalous magnetic moments. The results are plotted for several values of light quark mass $m_l(0)$ (for simplicity we denote it by m_0) and $m_s(0) = m_l(0) + 120$ MeV. (b) The effect of anomalous magnetic moments ($m_l(0) = 600$ MeV). (c) Anatomy of $\chi_B(T) - \chi_B(0)$ ($m_l(0) = 600$ MeV, $\kappa_q \neq 0$). In all panels $\Lambda = 800$ MeV.

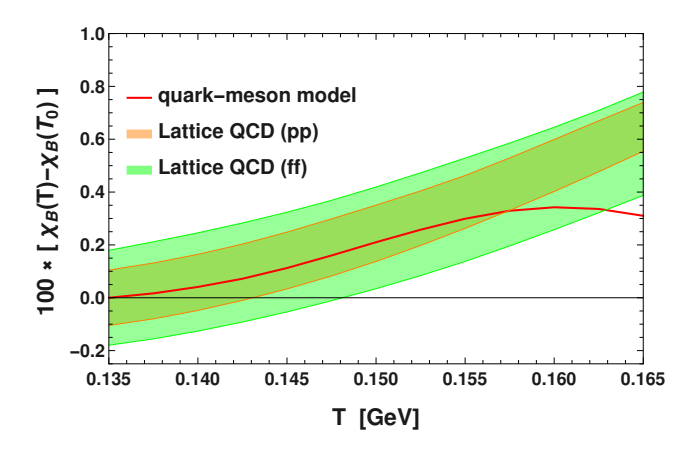


FIG. 9. Same as in Fig. 1, but for $\chi_B(T) - \chi_B(T_0)$ with $T_0 = 135$ MeV where the lattice data are represented as before and the red solid curve denotes he result from quark-meson model.

temperature dependence of χ_B (by construction, it also agrees with $\chi_{\mathcal{B}\mathcal{B}}$ ad $\chi_{\mathcal{B}S}$) but, admittedly, some only partially controlled parameters are introduced, such as the cut-off Λ , the mass of the quark at T=0 needed for the subtraction, or the anomalous magnetic moments of the quarks.

To avoid the dependence on the unknown quark mass at T=0, one can subtract the value of χ_B at a temperature within the range of the data in Fig. 1, for instance at $T_0=135$ MeV. We can thus evaluate $\chi_B(T)-\chi_B(T_0)$ and compare it with the similarly subtracted lattice data. In Fig. 9, we show the result of such a prescription. It can be seen that the quark-meson model reproduces the lattice data reasonably well up to $T\sim155$ MeV.

VI. PION-VECTOR-MESON LOOPS

In the last part of this paper we return to a purely hadronic description to explore yet another contribution to the paramagnetism of the medium, which originates from the pion–vector-meson loops in the photon polarization. The possibility of couplings between photons, pions, and vector mesons involving the Levi-Civita tensor $\epsilon^{\alpha\beta\mu\nu}$ is well known, and such "anomalous" effects are expected to be generically small. Yet, it is worthwhile to examine the issue in a great detail to have a complete picture.

In analogy to Eq. (28) [4, 9, 73, 74],

$$\chi_B = \frac{1}{2} \lim_{q \to 0} \lim_{q_0 \to 0} \frac{\partial^2 \text{Re}[\Pi_s]}{\partial q^2} , \qquad (34)$$

To pick up the thermal contribution, one calculates the vacuum polarization tensor of the photon using the loop diagrams, where one of the propagators in the loop corresponds to the thermal part. For the case where the two propagators in the loop correspond to the same particle,

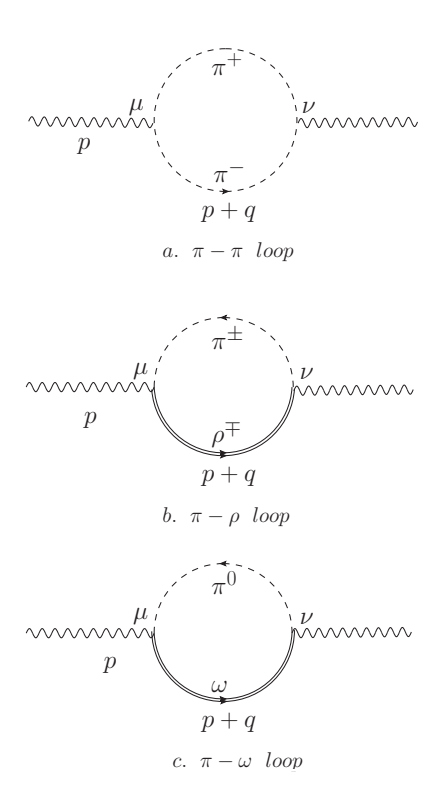


FIG. 10. Vacuum polarization diagrams for photons, involving a π loop (a) and π -vector-meson loops, (b) and (c).

such as for instance the pion, one obtains the formula of Eq. (23) as a check.

The loops, however, can mix different states. In particular, there is the above-mentioned coupling between a photon, pion, and a vector meson (cf. Fig. 10). A detailed calculation of these diagrams is provided in Appendix C 2. The magnetic susceptibility in this case becomes,

$$\chi_B = -\frac{1}{12\pi^2 \Delta} \left(\frac{g_{\gamma\pi V}^2}{m_V^2} \right) [I_{\pi} - I_V],$$
(35)

where $V = \rho, \omega$, $\Delta = m_V^2 - m_\pi^2$, $g_{\gamma\pi V}$ is the coupling constant, and I_a is given by,

$$I_a = \int p^2 dp \frac{f(E_a)}{E_a} (p^2 - 3E_a), \quad a = \pi, V.$$
 (36)

Here $E_a = \sqrt{p^2 + m_a^2}$ represents the energy of meson a. The values of the coupling constants have been determined from the vector meson electroproduction data and have the values [81, 82]

$$g_{\gamma\pi\rho} = 0.54, \quad g_{\gamma\pi\omega} = 1.82.$$
 (37)

In Eq. (35), I_{π} dominates over I_{V} due to the small mass of the pion compared to the masses of ρ or ω .

Fig. 11 shows that the contribution of the pion–vectormeson loops to χ_B is indeed small. To assess the effect, we use the HRG result from Fig. 2. It can be seen that

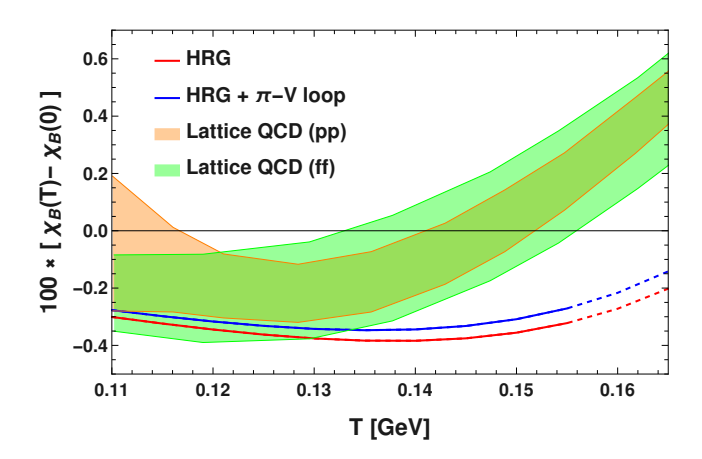


FIG. 11. Magnetic susceptibility as a function of temperature in usual HRG (red) and HRG with the contribution coming from anomalous coupling such as $\rho-\pi$ and $\pi-\omega$ loops in the vacuum polarization of γ (blue), compared with lattice data (orange).

the mixing effect is strictly paramagnetic and moderate, ranging from 10% to 20% while going from low to high temperatures. Nevertheless, it should be noted that the $\pi-\rho$ contribution is larger than the $\rho-\rho$ contribution, hence carries some significance. Notably, the sign and the order of magnitude of the enhancement from the pionvector-meson loops is in a quantitative agreement with a two-loop chiral perturbation theory calculation [54].

VII. CONCLUSIONS

Here are the main results of this paper:

- Within HRG, it is impossible to describe simultaneously the lattice data for the conserved charge susceptibilities, $\chi_{\mathcal{BB}}$ and $\chi_{\mathcal{BS}}$, and the magnetic susceptibility, $\chi_{\mathcal{B}}$. In the fiducial range of temperatures where HRG should apply, there is a general need for paramagnetism provided by some relatively light states (such as constituent quarks). Pions are a necessary ingredient to account for the diamagnetic contribution at low temperatures.
- We have explored a framework of non-interacting quarks and mesons (pions and kaons) to simultaneously describe the lattice data for the conserved charge multiplicities and for χ_B in the vicinity of T_c . In this picture, fitting the lattice results for χ_{BB} and χ_{BS} yields the effective temperature-dependent quark masses above the typical constituent values, but, interestingly, very close to the quasi-particle description [71].
- The vacuum contribution to the pressure does not directly affect the conserved charge susceptibilities, but it does contribute to χ_B . Our modeling incorporates the vacuum contribution from quark loops,

treated with a low-energy cut-off, and from meson loops.

- We have accounted for the anomalous magnetic moments of the quarks, which improve the results.
- The contribution of the hadron magnetic polarizabilities to the magnetic susceptibility is negligible.
- In the hadronic picture, the contribution to the magnetic susceptibility arising from the pion-vector-meson loops in the photon vacuum is paramagnetic and small.

ACKNOWLEDGMENTS

The authors acknowledge the support from the Polish National Science Center grant 2023/51/B/ST2/01625.

Appendix A: χ_B in HRG

1.
$$\kappa = 0$$
 case

The expression for the pressure of Eq. 8 at $\kappa=0$ becomes

$$P = \eta T \frac{B|Q|}{2\pi^2} \sum_{l=0}^{\infty} \sum_{s_z=-s}^{s} \int_0^{\infty} dp_z$$
 (A1)

$$\log \left[1 + \eta \exp(-\frac{\sqrt{M^2 + p_z^2 + B[|Q|(2l+1) - 2Qs_z]}}{T})\right].$$

Next, applying Euler-Mclaurin summation formula [59],

$$\sum_{l=0}^{\infty} f(l + \frac{1}{2}) \simeq \int_{0}^{\infty} f(x)dx + \frac{1}{24}f'(0)$$
 (A2)

and using scaled variables $p_z = rM$, T = tM and $x = z^2M^2/2B|Q|$, one obtains

$$\chi_B = \frac{\partial^2 P}{\partial B^2} \bigg|_{B=0} = \frac{Q^2}{2\pi^2} \left(\sum_{s_z = -s}^s s_z^2 \right) \times$$

$$\int_0^\infty dr \int_0^\infty dz \ z \frac{(t + S(r, z)) \exp(\frac{S(r, z)}{t}) + \eta \ t}{t \ S(r, z)^3 \left(\exp(\frac{S(r, z)}{t}) + \eta \right)^2}$$

$$-\frac{Q^2}{24\pi^2} \sum_{s_z = -s}^s \int_0^\infty dr \frac{1}{S(r, 0) \left(\exp(\frac{S(r, 0)}{t}) + \eta \right)} \ , \tag{A3}$$

where $S(r,z)=\sqrt{1+r^2+z^2}$. The first term is paramagnetic (positive) and the second is diamagnetic (negative). Writing them as χ_B^{para} and χ_B^{dia} we obtain

$$\chi_B^{dia} = -\frac{Q^2(2s+1)}{24\pi^2} \int_0^\infty dp \frac{f(E_p)}{E_p}, \tag{A4}$$

where $E_p = \sqrt{p^2 + m^2}$ and $f(E_p)$ is the distribution function. Similarly, the paramagnetic term can be calculated by carrying out the z-integration and an integration by parts,

$$\chi_B^{para} = \frac{Q^2 s(s+1)(2s+1)}{6\pi^2} \int_0^\infty dp \, \frac{f(E_p)}{E_p}. (A5)$$

Comparing with the diamagnetic part we have,

$$\frac{\chi_B^{para}}{\chi_B^{dia}} = -4s(s+1),\tag{A6}$$

which for spin- $\frac{1}{2}$ states yields -3.

2.
$$\kappa \neq 0$$
 case

For $\kappa \neq 0$ case, the diamagnetic contribution remains of course the same. The paramagnetic part depends on the spin of the particle. Let us first consider the Tsai-Yildiz formula of Eq. (17) for spin- $\frac{1}{2}$ particles. Carrying out similar steps as in the $\kappa=0$ case, we find the term linear in κ ,

$$\frac{\kappa \frac{Qs(s+1)(2s+1)}{3\pi^2} \int dz \int dr}{z \left(e^{\frac{S(r,z)}{t}} \left(-r^2t + S(0,z)^2 S(r,z)\right) - r^2 t\eta\right)}{tS(0,z)S(r,z)^3 \left(e^{\frac{S(r,z)}{t}} + \eta\right)^2}, (A7)$$

and quadratic in κ ,

$$\frac{\kappa^2 \frac{s(s+1)(2s+1)}{6\pi^2} \int dr \int dz}{z \left(e^{\frac{S(r,z)}{t}} S(0,z)^4 S(r,z) - r^2 t S(0,z)^2 \left(e^{\frac{S(r,z)}{t}} + \eta\right)\right)}{t S(0,z)^2 S(r,z)^3 \left(e^{\frac{S(r,z)}{t}} + \eta\right)^2}.$$

which after carrying out the z-integration and integration by parts over r lead to Eq. (24). Similarly using the energy expression for higher spin particles in Eq. (20), one obtains Eq. (A10).

For spin-1 or $\frac{3}{2}$ particles, with Eq. (20) the paramagnetic contribution is given by

$$\chi_{B;s=1,\frac{3}{2}}^{para} = \frac{s(s+1)(2s+1)}{6\pi^2} \int_0^\infty dp \times$$

$$\left[Q^2 + 2Q \left(1 + \frac{p^2}{m^2} \right)^{1/2} \kappa + \left(1 + 2\frac{p^2}{m^2} \right) \kappa^2 \right] \frac{f(E_p)}{E_p}.$$

Similarly, using the expression for higher spin particles using Eq. (21) one arrives at

$$\chi_{B;s>\frac{3}{2}}^{para} = \frac{s(s+1)(2s+1)(Q+\kappa)^2}{6\pi^2} \times \qquad (A10)$$
$$\int_0^\infty dp \left(1 + 2\frac{p^2}{m^2}\right) \frac{f(E_p)}{E_p}.$$

Appendix B: Vacuum contribution to χ_B from quark loops

We consider non-zero anomalous magnetic moment of quarks. In presence of κ , the photon vacuum polarization tensor is given by

$$\Pi^{\mu\nu} = ie^2 \int \frac{d^4p}{(2\pi)^4} \operatorname{Tr}[\Gamma^{\mu} S_F(p+q) \Gamma^{\nu} S_F(p)], (B1)$$

where $\Gamma^{\mu} = Q \gamma^{\mu} + \frac{\kappa}{2M} \sigma^{\mu\nu} q^{\nu}$, with $\sigma^{\mu\nu} = -\frac{i}{4} [\gamma^{\mu}, \gamma^{\nu}]$. $p = (p_0, \vec{p})$ and $q = (q_0, \vec{q})$ are the loop momentum and the external momentum respectively. $S_F(p)$ denotes the vacuum quark propagator

$$S_F(p) = \frac{\not p + m}{p^2 - m^2 + i\epsilon}.$$
 (B2)

Using Eq. (28) yields

$$\chi_B^{\text{vac}} = R_0 + R_1 \kappa + R_2 \kappa^2, \tag{B3}$$

where

$$R_0 = \frac{4}{3}Q^2\pi^2 \left[(q^2 + 2m^2)B_0(q^2, m^2, m^2) - 2A_0(m^2) \right],$$

$$R_1 = 4\pi^2 Q \ q^2 B_0(q^2, m^2, m^2), \tag{B4}$$

$$R_2 = \frac{\pi^2}{6} \frac{q^2}{M^2} \left[(q^2 + 8m^2)B_0(q^2, m^2, m^2) - 2A_0(m^2) \right].$$

Here A_0 and B_0 are the one-loop Passarino-Veltman (PaVe) functions [83],

$$i\pi^{2}A_{0}(m^{2}) = \int d^{4}p \, \frac{1}{p^{2} - m^{2} + i\epsilon},$$

$$i\pi^{2}B_{0}(q^{2}, m_{1}^{2}, m_{2}^{2}) = \int d^{4}p \, \left[\frac{1}{(p+q)^{2} - m_{1}^{2} + i\epsilon} \frac{1}{p^{2} - m_{2}^{2} + i\epsilon} \right].$$
(B5)

Since these integrals are divergent, one needs to use regularization. In an effective model, regularization has a meaning of suppressing the high-momentum contributions in the loop integration. Here we use Pauli-Villars regularization of [52, 53] using two subtractions, amounting to the replacement of $F(\{m^2\})$ with

$$F^{\Lambda}(\{m^2\}) = F(\{m^2\}) - F(\{m^2 + \Lambda^2\}) + \Lambda^2 \frac{dF(\{M^2 + \Lambda^2\})}{d\Lambda^2},$$
 (B6)

where F denotes a PaVe function. We explicitly obtain

$$A_0 = -\frac{m^2 \log(\frac{m^2}{\Lambda^2 + m^2}) + \Lambda^2}{16\pi^4}$$

$$B_0 = \frac{\log(\frac{\Lambda^2}{m^2} + 1) - \frac{\Lambda^2}{\Lambda^2 + m^2}}{16\pi^4} + \frac{\Lambda^4 q^2}{96\pi^4 m^2 (\Lambda^2 + m^2)^2}.$$
(B7)

After collecting the terms in Eq. (B3) we obtain Eq. (31).

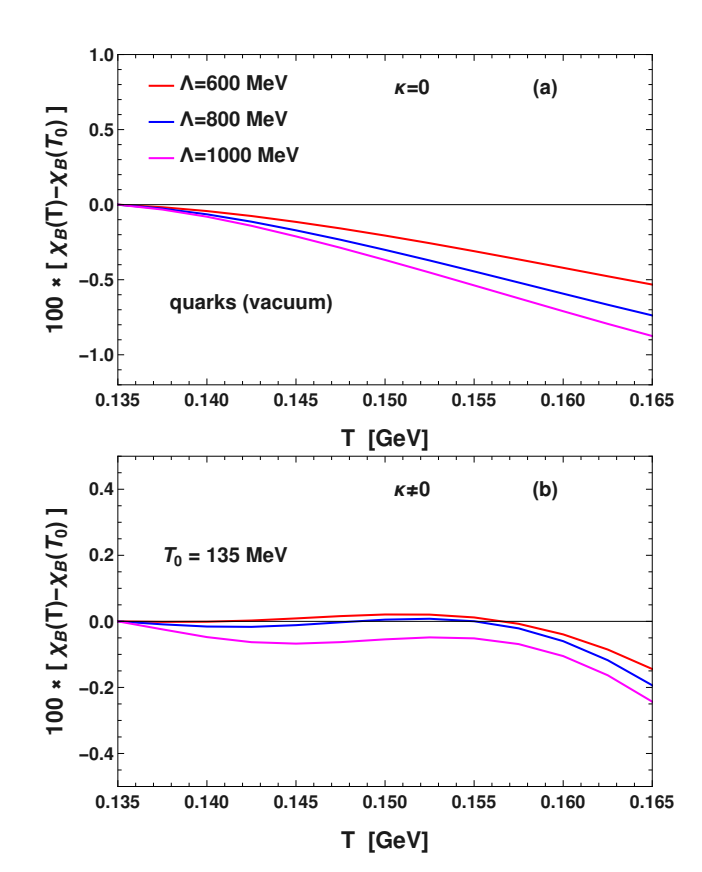


FIG. 12. Vacuum quark contribution to χ_B as a function of temperature for different values of the regulator Λ , with $\kappa = 0$ (a) and $\kappa \neq 0$ (b).

Lattice QCD presents the results for χ_B subtracted at T=0. In the absence of precise knowledge about m(T=0) from our fit to the lattice data for $\chi_{\mathcal{BB}}$ and $\chi_{\mathcal{BS}}$, we can subtract the value at $T_0=135$ MeV. The results are presented in Fig. 12 for different values of Λ , both for $\kappa=0$ and non-zero. Formally, the $\Lambda\to\infty$ limit for $\kappa=0$ reproduces the result of [4, 48], which may serve as a check.

Appendix C: Pion-vector meson loop contributions to χ_B

1.
$$\pi - \pi$$
 loop

As a warm up, let us first consider the case where the photon vacuum polarization diagram involves a pion loop as drawn in Fig. 10(a). The polarization tensor is

$$\Pi^{\mu\nu} = -ie^2 \int \frac{d^4p}{(2\pi)^4} (2p+q)^{\mu} S_B(p+q) (2p+q)^{\nu} S_B(p),$$
(C1)

where the thermal propagator $S_B(p)$ is given by

$$S_B(p) = \frac{1}{p^2 - m^2 + i\epsilon} - 2\pi i f(|p_0|)\delta(p^2 - m^2).$$
 (C2)

Here f is the Bose-Einstein distribution function of Eq. 6.

The magnetic susceptibility is defined by Eq. 28 [9]. After plugging in the propagator in Eq. C2 inside Eq. C1, taking the limit $q_0 \to 0$, and carrying out the sum over the spatial index, one obtains

$$\lim_{q_0 \to 0} \Pi_s^{T \neq 0} = -\pi e^2 \int \frac{d^3 p}{(2\pi)^3} \frac{dp_0}{2\pi} f(|p_0|) \delta(p_0^2 - E_p^2)$$

$$\left[\frac{q^2 + 4p^2 + 4\vec{q} \cdot \vec{p}}{p_0^2 - E_p^2 - q^2 - 2\vec{p} \cdot \vec{q} + i\epsilon} + \frac{q^2 + 4p^2 - 4\vec{q} \cdot \vec{p}}{p_0^2 - E_p^2 - q^2 + 2\vec{p} \cdot \vec{q} + i\epsilon} \right].$$
(C3)

Performing the delta function integral and taking only the positive-energy contribution one gets

$$\lim_{q_0 \to 0} \Pi_s^{T \neq 0} = -\frac{e^2}{16\pi^2} \int p^2 dp \frac{f(E_p)}{E_p}$$

$$\int_{-1}^{+1} dz \left[\frac{q^2 + 4p^2 + 4qpz}{-q^2 - 2qpz + i\epsilon} + \frac{q^2 + 4p^2 - 4qpz}{-q^2 + 2qpz + i\epsilon} \right] (C4)$$

Taking the real part of the above equation, carrying out the z-integration, and taking the limit $\epsilon \to 0$ yields

$$\lim_{q_0 \to 0} \operatorname{Re}[\Pi_s^{T \neq 0}] = \frac{e^2}{16\pi^2} \int p^2 dp \frac{f(E_p)}{E_p} \times \left[8 + \frac{q^2 - 4p^2}{q \ p} \log \left[\frac{q - 2p}{q + 2p} \right] \right]. \tag{C5}$$

Finally, by applying Eq. (34) one arrives at Eq. (23).

Following similar methods for the fermions, one obtains Eq. (25).

2. χ_B from π -vector-meson loop

Similarly as in the previous subsection, one can calculate the vacuum polarization diagram of $\pi - V$ loop as drawn in Fig. 10(b,c). The only differences are that now we have a different coupling at the vertices due to involvement of a vector boson and two bosons involved within the loop have different masses, m_{π} and m_{V} . The polarization tensor in this case is given by,

$$\Pi^{\mu\nu} = -ie^2 \left(\frac{g^2}{m_V^2}\right) \int \frac{d^4p}{(2\pi)^4} G^{\mu\nu}(p,q) S_B^{\pi}(p+q) S_B^V(p),$$
(C6)

where

$$G^{\mu\nu}(p,q) = \varepsilon^{p\alpha q\mu} \left(\frac{p^{\alpha}p^{\beta}}{m_V^2} - g^{\alpha\beta}\right) \varepsilon^{p\beta q\nu}$$
 and $\varepsilon^{p\alpha q\mu} = \varepsilon_{\gamma\alpha\delta\mu} p^{\gamma} q^{\delta}$. This yields

$$\Pi_s^{T\neq 0} = -\pi e^2 \left(\frac{g^2}{m_V^2}\right) \int \frac{d^4 p}{(2\pi)^4} \times \left[\sum_{i=1}^3 G^{ii}(p,q) f(|p_0|) \frac{\delta(p^2 - m_V^2)}{(p+q)^2 - m_\pi^2 + i\epsilon} + \sum_{i=1}^3 G^{ii}(p-q,q) f(|p_0|) \frac{\delta(p^2 - m_\pi^2)}{(p-q)^2 - m_V^2 + i\epsilon}\right] (C8)$$

and

$$\lim_{q_0 \to 0} \operatorname{Re}[\Pi_s^{T \neq 0}] = -\frac{e^2}{16\pi^2} \left(\frac{g^2}{m_V^2}\right) \int p^2 dp \int_{-1}^{+1} dz \times \operatorname{Re}\left[\frac{f(E_V)}{E_V} \frac{q^2(p^2 z^2 - p^2 + 2E_V^2)}{\Delta - q^2 - 2qpz + i\epsilon} + \frac{f(E_\pi)}{E_\pi} \frac{q^2(p^2 z^2 - p^2 + 2E_\pi^2)}{-\Delta - q^2 + 2qpz + i\epsilon}\right]$$
(C9)

where $\Delta = m_V^2 - m_\pi^2$. Following similar steps as in the previous subsection yields Eq. (35).

- [1] G. S. Bali, F. Bruckmann, G. Endrodi, Z. Fodor, S. D. Katz, S. Krieg, A. Schafer, and K. K. Szabo, The QCD phase diagram for external magnetic fields, JHEP 02, 044, arXiv:1111.4956 [hep-lat].
- [2] G. S. Bali, F. Bruckmann, M. Constantinou, M. Costa, G. Endrodi, S. D. Katz, H. Panagopoulos, and A. Schafer, Magnetic susceptibility of QCD at zero and at finite temperature from the lattice, Phys. Rev. D 86, 094512 (2012), arXiv:1209.6015 [hep-lat].
- [3] M. D'Elia, Lattice QCD Simulations in External Background Fields, Lect. Notes Phys. 871, 181 (2013), arXiv:1209.0374 [hep-lat].
- [4] G. Endrödi, QCD equation of state at nonzero magnetic fields in the Hadron Resonance Gas model, JHEP 04, 023, arXiv:1301.1307 [hep-ph].

- [5] C. Bonati, M. D'Elia, M. Mariti, F. Negro, and F. Sanfilippo, Magnetic Susceptibility of Strongly Interacting Matter across the Deconfinement Transition, Phys. Rev. Lett. 111, 182001 (2013), arXiv:1307.8063 [hep-lat].
- [6] C. Bonati, M. D'Elia, M. Mariti, F. Negro, and F. Sanfilippo, Magnetic susceptibility and equation of state of $N_f = 2+1$ QCD with physical quark masses, Phys. Rev. D **89**, 054506 (2014), arXiv:1310.8656 [hep-lat].
- [7] G. S. Bali, F. Bruckmann, G. Endrödi, S. D. Katz, and A. Schäfer, The QCD equation of state in background magnetic fields, JHEP 08, 177, arXiv:1406.0269 [hep-lat].
- [8] G. S. Bali, G. Endrődi, and S. Piemonte, Magnetic susceptibility of QCD matter and its decomposition from the lattice, JHEP 07, 183, arXiv:2004.08778 [hep-lat].

- [9] G. Endrődi and G. Markó, On electric fields in hot QCD: perturbation theory, JHEP 12, 015, arXiv:2208.14306 [hep-ph].
- [10] H.-T. Ding, J.-B. Gu, A. Kumar, S.-T. Li, and J.-H. Liu, Baryon Electric Charge Correlation as a Magnetometer of QCD, Phys. Rev. Lett. 132, 201903 (2024), arXiv:2312.08860 [hep-lat].
- [11] G. Endrodi, QCD with background electromagnetic fields on the lattice: A review, Prog. Part. Nucl. Phys. 141, 104153 (2025), arXiv:2406.19780 [hep-lat].
- [12] N. Astrakhantsev, V. V. Braguta, A. Y. Kotov, and A. A. Roenko, QCD equation of state at nonzero baryon density in an external magnetic field, Phys. Rev. D 109, 094511 (2024), arXiv:2403.07783 [hep-lat].
- [13] H.-T. Ding, J.-B. Gu, A. Kumar, and S.-T. Li, Second order fluctuations of conserved charges in external magnetic fields, Phys. Rev. D 111, 114522 (2025), arXiv:2503.18467 [hep-lat].
- [14] J. O. Andersen, W. R. Naylor, and A. Tranberg, Phase diagram of QCD in a magnetic field: A review, Rev. Mod. Phys. 88, 025001 (2016), arXiv:1411.7176 [hep-ph].
- [15] P. Adhikari et al., Strongly interacting matter in extreme magnetic fields, Prog. Part. Nucl. Phys. 146, 104199 (2026), arXiv:2412.18632 [nucl-th].
- [16] D. E. Kharzeev, L. D. McLerran, and H. J. Warringa, The Effects of topological charge change in heavy ion collisions: 'Event by event P and CP violation', Nucl. Phys. A 803, 227 (2008), arXiv:0711.0950 [hep-ph].
- [17] K. Fukushima, D. E. Kharzeev, and H. J. Warringa, The Chiral Magnetic Effect, Phys. Rev. D 78, 074033 (2008), arXiv:0808.3382 [hep-ph].
- [18] D. E. Kharzeev, J. Liao, S. A. Voloshin, and G. Wang, Chiral magnetic and vortical effects in high-energy nuclear collisions—A status report, Prog. Part. Nucl. Phys. 88, 1 (2016), arXiv:1511.04050 [hep-ph].
- [19] J. O. Andersen, QCD phase diagram in a constant magnetic background: Inverse magnetic catalysis: where models meet the lattice, Eur. Phys. J. A 57, 189 (2021), arXiv:2102.13165 [hep-ph].
- [20] F. Karsch and E. Laermann, Susceptibilities, the specific heat and a cumulant in two flavor QCD, Phys. Rev. D 50, 6954 (1994), arXiv:hep-lat/9406008.
- [21] C. Sasaki, B. Friman, and K. Redlich, Susceptibilities and the Phase Structure of a Chiral Model with Polyakov Loops, Phys. Rev. D 75, 074013 (2007), arXiv:hepph/0611147.
- [22] A. Bazavov et al., The chiral and deconfinement aspects of the QCD transition, Phys. Rev. D 85, 054503 (2012), arXiv:1111.1710 [hep-lat].
- [23] P. Adhikari and J. O. Andersen, Quark condensates and magnetization in chiral perturbation theory in a uniform magnetic field, (2021), arXiv:2102.01080 [hep-ph].
- [24] M. A. Stephanov, K. Rajagopal, and E. V. Shuryak, Signatures of the tricritical point in QCD, Phys. Rev. Lett. 81, 4816 (1998), arXiv:hep-ph/9806219.
- [25] Z. Fodor and S. D. Katz, Critical point of QCD at finite T and mu, lattice results for physical quark masses, JHEP 04, 050, arXiv:hep-lat/0402006.
- [26] Y. Aoki, G. Endrodi, Z. Fodor, S. D. Katz, and K. K. Szabo, The Order of the quantum chromodynamics transition predicted by the standard model of particle physics, Nature 443, 675 (2006), arXiv:hep-lat/0611014.
- [27] K. Fukushima and T. Hatsuda, The phase diagram of dense QCD, Rept. Prog. Phys. 74, 014001 (2011),

- arXiv:1005.4814 [hep-ph].
- [28] E. Fermi, High-energy nuclear events, Prog. Theor. Phys. 5, 570 (1950).
- [29] I. Y. Pomeranchuk, On the theory of multiple particle production in a single collision, Dokl. Akad. Nauk SSSR 78, 889 (1951).
- [30] R. Hagedorn, Statistical thermodynamics of strong interactions at high-energies, Nuovo Cim. Suppl. 3, 147 (1965).
- [31] P. Koch, B. Muller, and J. Rafelski, Strangeness in Relativistic Heavy Ion Collisions, Phys. Rept. 142, 167 (1986).
- [32] R. Dashen, S.-K. Ma, and H. J. Bernstein, S Matrix formulation of statistical mechanics, Phys. Rev. 187, 345 (1969).
- [33] R. Venugopalan and M. Prakash, Thermal properties of interacting hadrons, Nucl. Phys. A 546, 718 (1992).
- [34] F. Karsch, K. Redlich, and A. Tawfik, Thermodynamics at nonzero baryon number density: A Comparison of lattice and hadron resonance gas model calculations, Phys. Lett. B 571, 67 (2003), arXiv:hep-ph/0306208.
- [35] M. Gyulassy and L. McLerran, New forms of QCD matter discovered at RHIC, Nucl. Phys. A 750, 30 (2005), arXiv:nucl-th/0405013.
- [36] P. Huovinen and P. Petreczky, QCD Equation of State and Hadron Resonance Gas, Nucl. Phys. A 837, 26 (2010), arXiv:0912.2541 [hep-ph].
- [37] A. Bazavov et al. (HotQCD), Equation of state in (2+1)-flavor QCD, Phys. Rev. D 90, 094503 (2014), arXiv:1407.6387 [hep-lat].
- [38] H.-T. Ding, F. Karsch, and S. Mukherjee, Thermodynamics of strong-interaction matter from Lattice QCD, Int. J. Mod. Phys. E 24, 1530007 (2015), arXiv:1504.05274 [hep-lat].
- [39] S. Borsanyi, Z. Fodor, S. D. Katz, S. Krieg, C. Ratti, and K. Szabo, Fluctuations of conserved charges at finite temperature from lattice QCD, JHEP 01, 138, arXiv:1112.4416 [hep-lat].
- [40] A. Bazavov et al. (HotQCD), Fluctuations and Correlations of net baryon number, electric charge, and strangeness: A comparison of lattice QCD results with the hadron resonance gas model, Phys. Rev. D 86, 034509 (2012), arXiv:1203.0784 [hep-lat].
- [41] R. Bellwied, S. Borsanyi, Z. Fodor, S. D. Katz, A. Pasztor, C. Ratti, and K. K. Szabo, Fluctuations and correlations in high temperature QCD, Phys. Rev. D 92, 114505 (2015), arXiv:1507.04627 [hep-lat].
- [42] S. Borsanyi, Z. Fodor, J. N. Guenther, S. K. Katz, K. K. Szabo, A. Pasztor, I. Portillo, and C. Ratti, Higher order fluctuations and correlations of conserved charges from lattice QCD, JHEP 10, 205, arXiv:1805.04445 [hep-lat].
- [43] D. Bollweg, J. Goswami, O. Kaczmarek, F. Karsch, S. Mukherjee, P. Petreczky, C. Schmidt, and P. Scior (HotQCD), Second order cumulants of conserved charge fluctuations revisited: Vanishing chemical potentials, Phys. Rev. D 104, 10.1103/PhysRevD.104.074512 (2021), arXiv:2107.10011 [hep-lat].
- [44] H. T. Ding, S. T. Li, Q. Shi, and X. D. Wang, Fluctuations and correlations of net baryon number, electric charge and strangeness in a background magnetic field, Eur. Phys. J. A 57, 202 (2021), arXiv:2104.06843 [hep-lat].
- [45] R. Samanta and W. Broniowski, Magnetic properties of the hadron resonance gas with physical mag-

- netic moments, Phys. Rev. C 112, 045202 (2025), arXiv:2505.14484 [hep-ph].
- [46] A. Andronic, P. Braun-Munzinger, K. Redlich, and J. Stachel, Decoding the phase structure of QCD via particle production at high energy, Nature 561, 321 (2018), arXiv:1710.09425 [nucl-th].
- [47] B. B. Brandt, G. Endrődi, G. Markó, and A. D. M. Valois, Steady electric currents in magnetized QCD and their use for the equation of state, JHEP 07, 027, arXiv:2405.06557 [hep-lat].
- [48] K. Kamikado and T. Kanazawa, Magnetic susceptibility of a strongly interacting thermal medium with 2+1 quark flavors, JHEP 01, 129, arXiv:1410.6253 [hep-ph].
- [49] L. McLerran, K. Redlich, and C. Sasaki, Quarkyonic Matter and Chiral Symmetry Breaking, Nucl. Phys. A 824, 86 (2009), arXiv:0812.3585 [hep-ph].
- [50] L. McLerran and S. Reddy, Quarkyonic Matter and Neutron Stars, Phys. Rev. Lett. 122, 122701 (2019), arXiv:1811.12503 [nucl-th].
- [51] M. Marczenko, L. McLerran, K. Redlich, and C. Sasaki, Reaching percolation and conformal limits in neutron stars, Phys. Rev. C 107, 025802 (2023), arXiv:2207.13059 [nucl-th].
- [52] E. Ruiz Arriola, Pion structure at high-energies and low-energies in chiral quark models, Acta Phys. Polon. B 33, 4443 (2002), arXiv:hep-ph/0210007.
- [53] W. Broniowski, E. Ruiz Arriola, and P. Sanchez-Puertas, Baryonic form factors of the pion and kaon in a chiral quark model, Phys. Rev. D 106, 036001 (2022), arXiv:2112.11049 [hep-ph].
- [54] C. P. Hofmann, Diamagnetic and paramagnetic phases in low-energy quantum chromodynamics, Phys. Lett. B 818, 136384 (2021), arXiv:2103.04937 [hep-ph].
- [55] M. Marczenko, M. Szymański, P. M. Lo, B. Karmakar, P. Huovinen, C. Sasaki, and K. Redlich, Magnetic effects in the hadron resonance gas, Phys. Rev. C 110, 065203 (2024), arXiv:2405.15745 [hep-ph].
- [56] V. Vovchenko, Magnetic field effect on hadron yield ratios and fluctuations in a hadron resonance gas, Phys. Rev. C 110, 034914 (2024), arXiv:2405.16306 [hep-ph].
- [57] P. Huovinen, M. Marczenko, M. Szymański, B. Karmakar, P. M. Lo, C. Sasaki, and K. Redlich, Hadron resonance gas is not a good model for hadronic matter in a strong magnetic field, In: 31st International Conference on Ultra-relativistic Nucleus-Nucleus Collisions (2025) arXiv:2510.01431 [hep-ph].
- [58] L. D. Landau and E. M. Lifshitz, Statistical Physics, Part 1, Course of Theoretical Physics, Vol. 5 (Butterworth-Heinemann, Oxford, 1980).
- [59] R. K. Pathria and P. D. Beale, <u>Statistical Mechanics</u>, 3rd ed. (Elsevier/Academic Press, <u>Amsterdam</u>; Boston, 2011).
- [60] W. Broniowski and W. Florkowski, Explanation of the RHIC p(T) spectra in a thermal model with expansion, Phys. Rev. Lett. 87, 272302 (2001), arXiv:nuclth/0106050.
- [61] W.-Y. Tsai and A. Yildiz, Motion of charged particles in a homogeneous magnetic field, Phys. Rev. D 4, 3643 (1971).
- [62] M. G. de Paoli, D. P. Menezes, L. B. Castro, and C. C. Barros, Jr, The Rarita-Schwinger Particles Under de Influence of Strong Magnetic Fields, J. Phys. G 40, 055007 (2013), arXiv:1207.4063 [math-ph].

- [63] S. Pal, Strongly interacting matter under extreme conditions (2023), arXiv:2501.13123 [nucl-th].
- [64] W. Broniowski, W. Florkowski, and L. Y. Glozman, Update of the Hagedorn mass spectrum, Phys. Rev. D 70, 117503 (2004), arXiv:hep-ph/0407290.
- [65] M. Moinester, Pion Polarizability 2022 Status Report (2022) arXiv:2205.09954 [hep-ph].
- [66] F. He, D. B. Leinweber, A. W. Thomas, and P. Wang, Chiral extrapolation of the magnetic polarizability of the neutral pion, Phys. Rev. D 102, 114509 (2020), arXiv:2010.01580 [nucl-th].
- [67] S. Navas et al. (Particle Data Group), Review of particle physics, Phys. Rev. D 110, 030001 (2024).
- [68] B.-J. Schaefer and J. Wambach, The Phase diagram of the quark meson model, Nucl. Phys. A 757, 479 (2005), arXiv:nucl-th/0403039.
- [69] S. Mao, Correlations and fluctuations in a magnetized PNJL model with and without the inverse magnetic catalysis effect, Chin. Phys. C 49, 063106 (2025), arXiv:2410.10217 [hep-ph].
- [70] J. Mei, R. Wen, S. Mao, M. Huang, and K. Xu, Magnetic catalysis and diamagnetism from pion fluctuations, Phys. Rev. D 110, 034024 (2024), arXiv:2402.19193 [hep-ph].
- [71] V. Mykhaylova, M. Bluhm, K. Redlich, and C. Sasaki, Quark-flavor dependence of the shear viscosity in a quasiparticle model, Phys. Rev. D 100, 034002 (2019), arXiv:1906.01697 [hep-ph].
- [72] P. Chakraborty and J. I. Kapusta, Quasi-Particle Theory of Shear and Bulk Viscosities of Hadronic Matter, Phys. Rev. C 83, 014906 (2011), arXiv:1006.0257 [nucl-th].
- [73] H. A. Weldon, Covariant Calculations at Finite Temperature: The Relativistic Plasma, Phys. Rev. D 26, 1394 (1982).
- [74] Y. Fujimoto and H. Yamada, A supplementary remark on finite temperature perturbation, Z. Phys. C 37, 265 (1988).
- [75] P. J. A. Bicudo, J. E. F. T. Ribeiro, and R. Fernandes, The Anomalous magnetic moment of quarks, Phys. Rev. C 59, 1107 (1999), arXiv:hep-ph/9806243.
- [76] K. Xu, J. Chao, and M. Huang, Effect of the anomalous magnetic moment of quarks on magnetized QCD matter and meson spectra, Phys. Rev. D 103, 076015 (2021), arXiv:2007.13122 [hep-ph].
- [77] S. Ghosh, N. Chaudhuri, P. Roy, and S. Sarkar, Thermomagnetic modification of the anomalous magnetic moment of quarks using the NJL model, Phys. Rev. D 103, 116008 (2021), arXiv:2104.14112 [hep-ph].
- [78] W. Thirring, Electromagnetic properties of hadrons in the static s u6 model, in Quantum Electrodynamics, edited by P. Urban (Springer Vienna, Vienna, 1965) pp. 205–211.
- [79] G. Karl, Baryon magnetic moments and the spin of the proton, Phys. Rev. D 45, 247 (1992).
- [80] S. Capstick and B. D. Keister, Baryon magnetic moments in a relativistic quark model, (1996), arXiv:nuclth/9611055.
- [81] Y.-s. Oh, A. I. Titov, and T. S. H. Lee, Electromagnetic production of vector mesons at low-energies, in NSTAR2000: The Physics of Excited Nucleons (2000) pp. 255–262, arXiv:nucl-th/0004055.
- [82] A. Gokalp and O. Yilmaz, The Coupling constants g(rho pi gamma) and g(omega pi gamma) as derived from QCD sum rules, Eur. Phys. J. C 24, 117 (2002), arXiv:nuclth/0103033.

[83] G. Passarino and M. J. G. Veltman, One Loop Corrections for e+ e- Annihilation Into mu+ mu- in the Weinberg Model, Nucl. Phys. B $\bf 160$, 151 (1979).